JOURNAL OF GEOPHYSICAL RESEARCH, VOL. 117, D05115, doi:10.1029/2011JD016900, 2012

Comparison of gravity wave temperature variances from ray-based spectral parameterization of convective gravity wave drag with AIRS observations

Hyun-Joo Choi,[1] Hye-Yeong Chun,[1] Jie Gong,[2] and Dong L. Wu[2,3]

Received 20 September 2011; revised 28 December 2011; accepted 6 January 2012; published 8 March 2012.

[1] The realism of ray-based spectral parameterization of convective gravity wave drag, which considers the updated moving speed of the convective source and multiple wave propagation directions, is tested against the Atmospheric Infrared Sounder (AIRS) onboard the Aqua satellite. Offline parameterization calculations are performed using the global reanalysis data for January and July 2005, and gravity wave temperature variances (GWTVs) are calculated at $z = 2.5$ hPa (unfiltered GWTV). AIRS-filtered GWTV, which is directly compared with AIRS, is calculated by applying the AIRS visibility function to the unfiltered GWTV. A comparison between the parameterization calculations and AIRS observations shows that the spatial distribution of the AIRS-filtered GWTV agrees well with that of the AIRS GWTV. However, the magnitude of the AIRS-filtered GWTV is smaller than that of the AIRS GWTV. When an additional cloud top gravity wave momentum flux spectrum with longer horizontal wavelength components that were obtained from the mesoscale simulations is included in the parameterization, both the magnitude and spatial distribution of the AIRS-filtered GWTVs from the parameterization are in good agreement with those of the AIRS GWTVs. The AIRS GWTV can be reproduced reasonably well by the parameterization not only with multiple wave propagation directions but also with two wave propagation directions of 45° (northeast-southwest) and 135° (northwest-southeast), which are optimally chosen for computational efficiency.

Citation: Choi, H.-J., H.-Y. Chun, J. Gong, and D. L. Wu (2012), Comparison of gravity wave temperature variances from ray-based spectral parameterization of convective gravity wave drag with AIRS observations, *J. Geophys. Res.*, *117*, D05115, doi:10.1029/2011JD016900.

1. Introduction

[2] Atmospheric gravity waves (GWs) have a crucial effect on the large-scale circulation of the middle atmosphere. The waves forced by tropospheric sources such as mountains, convections, and jet front systems propagate upward and then force the circulation through momentum and energy transports to the large-scale flows when they dissipate (see *McLandress* [1998] for a review of the dynamics of the middle atmosphere and GWs). Although some GWs may be resolved in general circulation models (GCMs), the impacts of unresolved scale waves must be treated via parameterization of the GW drag (GWD) in the GCMs (see *Kim et al.* [2003] for a review of GWD parameterizations).

[3] Among the aforementioned sources of GWs, convection is well known as a major nonstationary GW source that generates GWs over a broad spectral range. To include the effects of convective GWs in GCMs, the parameterizations of convective GW drag (CGWD) have been developed and improved continuously [*Chun and Baik*, 1998, 2002; *Beres*, 2004; *Song and Chun*, 2005, 2008; *Kim and Chun*, 2005; *Chun et al.*, 2008; *Choi and Chun*, 2011]. Although significant theoretical and technical advances have been achieved in CGWD parameterizations, their realism in relation to observations has not been fully explored. The parameterizations include some tunable free parameters (e.g., GW amplitude, wave propagation direction, convective forcing scale), which need to be constrained by observations.

[4] Recent satellite observations can be used for a realism test and can provide constraints of the CGWD parameterizations, as they produce synoptic-scale plots of GW properties related to convection [e.g., *Preusse et al.*, 2001; *Jiang et al.*, 2004b; *Ratnam et al.*, 2004; *Grimsdell et al.*, 2010; *Wright and Gille*, 2011]. For example, *Choi et al.* [2009] validated the realism of the CGWD parameterization of *Song and Chun* [2008] and addressed the limitation associated with a free parameter (i.e., wave propagation direction) included in the parameterization through a comparison with

[1]Department of Atmospheric Sciences, Yonsei University, Seoul, South Korea.
[2]Jet Propulsion Laboratory, California Institute of Technology, Pasadena, California, USA.
[3]Now at NASA Goddard Space Flight Center, Greenbelt, Maryland, USA.

0148-0227/12/2011JD016900

the measurement results of an Upper Atmosphere Research Satellite (UARS) Microwave Limb Sounder (MLS). However, each satellite instrument can only observe a limited portion of the full GW spectrum [*Wu et al.*, 2006; *Alexander et al.*, 2010]; hence, the parameterizations need to be constrained by multiple observations.

[5] Among satellite GW observing instruments (limb, sublimb, and nadir sounders), the nadir sounders (e.g., Atmospheric Infrared Sounder (AIRS), Advanced Microwave Sounding Unit-A (AMSU-A), and Special Sensor Microwave Imager Sounder (SSMIS)) are mostly sensitive to GWs with a relatively high frequency and short horizontal and long vertical wavelengths. In particular, AIRS has a high horizontal resolution ($\sim$13 km at the nadir), which makes it more favorable for detecting small-scale GWs. Recently, some studies have shown that strong stratospheric GW activities have been observed by AIRS over deep convective regions [*Grimsdell et al.*, 2010; *Hoffmann and Alexander*, 2010; *Gong et al.*, 2011]. AIRS measurements are believed to provide observational constraints for the parameterized convective GWs with high frequencies and short horizontal wavelengths.

[6] In this study, we test the realism of the ray-based CGWD parameterization of *Song and Chun* [2008] with the GW momentum flux spectrum updated in the work of *Choi and Chun* [2011] against the AIRS measurements reported by *Gong et al.* [2011]. For the test, offline calculations of the parameterization are performed by using the global reanalysis data for January and July 2005, and the GW temperature variance (GWTV) calculated from the parameterization is compared with that observed from AIRS in the stratosphere. The comparison reveals limitations of the CGWD parameterization, which are addressed on the basis of the findings from the mesoscale simulations performed by *Choi and Chun* [2011]. Although the parameterization in this study considers multiple wave propagation directions to represent more realistic GW effects, the parameterization with the minimum number of the wave propagation directions, being chosen for computational efficiency, is also tested for its realism.

[7] The paper is organized as follows. The AIRS observations as well as the CGWD parameterization and its offline simulations are described in section 2. Comparisons between the parameterization results from the offline simulations and the AIRS observations are presented in section 3. Issues associated with the wave propagation direction are also discussed in section 3. A summary and discussions are given in section 4.

2. Experimental Design

2.1. AIRS Observations

[8] AIRS, one of the six instruments onboard the Aqua satellite, is an infrared nadir sounder. Its radiance fluctuations are sensitive to temperature perturbations induced by GWs with high frequency and short horizontal wavelength. The instrument scans between $\pm$ 48.95° from the nadir in the cross-track direction every 2.667 s and produces 90 footprints on the ground in each scan. AIRS scan lines are approximately along the west-east direction at most latitudes because the satellite tracks are largely in the meridional direction. The diameter of AIRS beam widths is about 13 km for all view angles, and the high horizontal resolution makes AIRS favorably detect GWs with shorter horizontal wavelengths compared to other satellite instruments (e.g., AUSU-A, MLS, CRISTA). AIRS provides 2378 radiance channels in the wavelength ranges of 3.74–4.61 μm, 6.20–8.22 μm, and 8.8–15.4 μm. In this study, we only use AIRS GW temperature variances (GWTVs) at z = 2.5 hPa from channel 75 (CO_2 15 μm radiance emission band) for January and July 2005, in which GW signals associated with deep convections are clearly identified [see *Gong et al.*, 2011, Figures 5 and 6]. The observed GWTVs are averaged for ascending and descending orbits because there are no significant differences between the two. The AIRS GWTVs are further averaged across view angles of $\pm$ 48.95°, and the mean values are used for comparisons with the CGWD parameterization.

[9] *Gong et al.* [2011] applied a 7 point (i.e., 7 consecutive data points) running smooth window to each scan to derive the AIRS GW variance, and the smallest window (3 points) was used to infer the instrument noise. Figure 1a shows the GW visibility of AIRS observations as a function of cross-track (λ_Y) and vertical (λ_Z) wavelengths. The contours represent temperature amplitude (K) responded to a GW packet with an amplitude of 1 K after applying the 7 point window. Figure 1b shows the AIRS cross-track visibility, which is identical to *Gong et al.* [2011, Figure 2]. The visibility increases sharply when λ_Y becomes larger than the AIRS footprint size ($\sim$13 km), and the peak occurs near λ_Y = 100 km, which corresponds to the width of the 7 point running smoothing window. The valid range of AIRS visibility appears to be $\sim$40 km < λ_Y < 500 km. The AIRS visibility along the vertical direction is computed from the normalized convolution of the GW packet with the weighting function for channel 75 (Figure 1c). The vertical visibility shows that GWs with a λ_Z longer than the full width at half maximum (FWHM) of the weighting function, which is about 12 km, are detectable in AIRS. The visibility increases with the increase of λ_Z. The same visibility function is applied to GWTVs from our CGWD parameterization to facilitate direct comparisons.

[10] *Gong et al.* [2011] inferred GW zonal propagation direction by comparing GWTVs from east and west views on the basis of the facts that the AIRS visibility is independent of view angle and random sampling. AIRS observed variance is a convolution of AIRS weighting function and the real GW-induced perturbations. Therefore, AIRS east (west) view would observe larger variance if the GW is propagating westward (eastward) as the integration of GW variances along west (east) view is largely smeared out [see *Gong et al.*, 2011, Figure 1]. In our study, we compare the GWTVs and the preferred zonal GW propagation direction between the parameterization and AIRS observations. The difference in AIRS GWTVs between the west view (averaged over $-$48.95° and 0°) and east view (averaged over 0° and 48.95°) is used to infer the prevailing GW direction. This is slightly different from *Gong et al.* [2011] where the outmost three angles are used in each west and east view, although the major conclusions do not alter.

[11] It is noteworthy that *Gong et al.* [2011, section 4.3] found a uniform belt of GW enhancement in the tropical lower stratosphere, and they suggested that this enhancement is induced by low-frequency inertial GWs with long

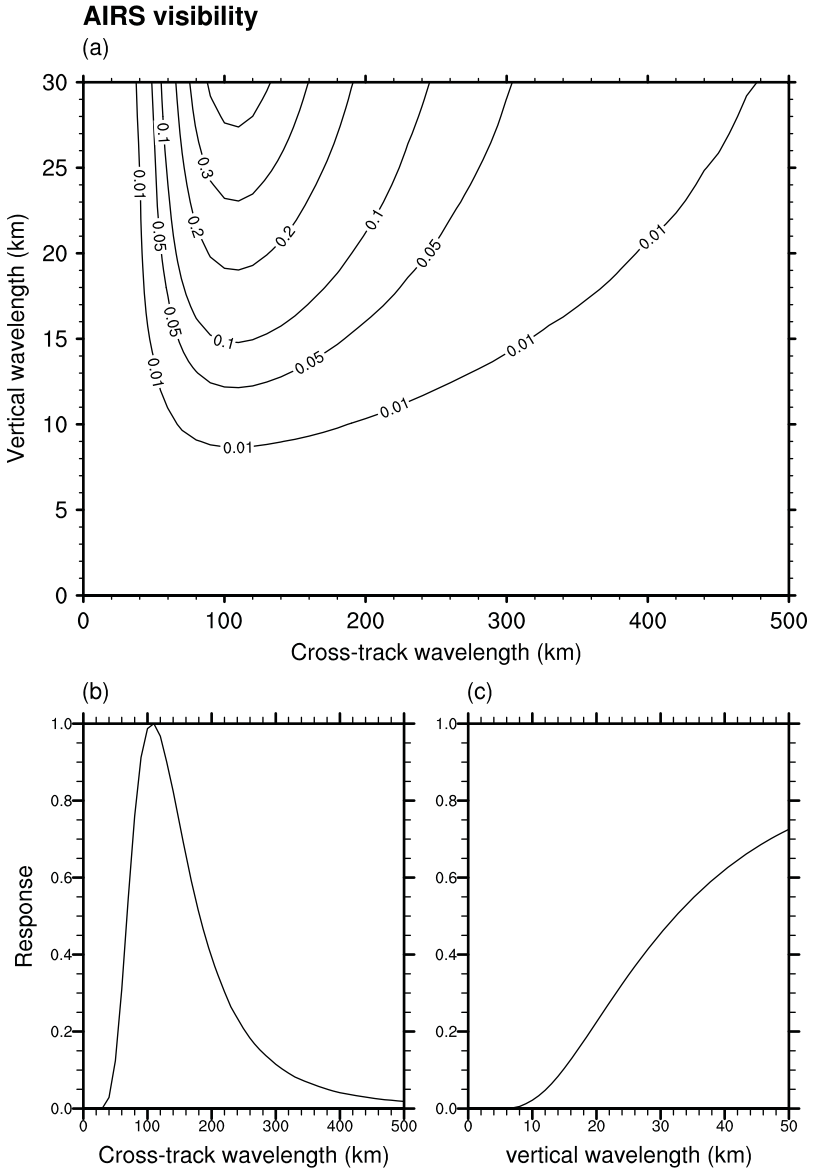

Figure 1. (a) Two-dimensional AIRS visibility with respect to the cross-track wavelength (λ_Y) and the vertical wavelength (λ_Z) after applying the 7 point window (see section 2.1), (b) AIRS cross-track visibility, and (c) AIRS vertical visibility. Contours in Figure 1a and response values in Figures 1b and 1c represent temperature amplitudes (K) responding to a GW packet with an amplitude of 1 K.

horizontal and short vertical wavelengths (best fit occurs at λ_Y = 700 km, λ_Z = 5 km). Because the convective GWs parameterized in the present study are the sub-grid-scale internal GWs, we add "background" GWTVs that represent inertial GWs to our parameterization results in order to directly compare with the AIRS observations. This will be discussed further in section 3.1.

2.2. CGWD Parameterization and Offline Simulation

[12] The CGWD parameterization used in this study is the ray-based spectral parameterization of *Song and Chun* [2008] with the GW momentum flux spectrum updated in the work of *Choi and Chun* [2011]. Offline calculations of the CGWD parameterization are performed by using deep convective heating (DCH) and background flow taken from the global reanalysis data sets for January and July 2005. The calculation procedure for the CGWD parameterization is composed of the following three parts.

[13] First, GW properties (e.g., wave numbers and frequencies) and the GW momentum flux spectrum are calculated at a reference level (cloud top). The cloud top GW momentum flux spectrum is analytically formulated as a function of phase speed (c) and wave propagation direction (φ) [*Song and Chun*, 2005] for a given diabatic forcing and basic state wind and stability in a three-layer atmosphere condition. The diabatic forcing is specified as a Gaussian-type structure in the horizontal direction and time. The spatial and temporal scales (δ_h and δ_t) of the forcing are set to 5 km and 20 min, respectively, on the basis of the mesoscale simulation by *Song et al.* [2003]. The magnitude of the diabatic forcing is determined by the maximum convective heating rate and adjusted by multiplying a

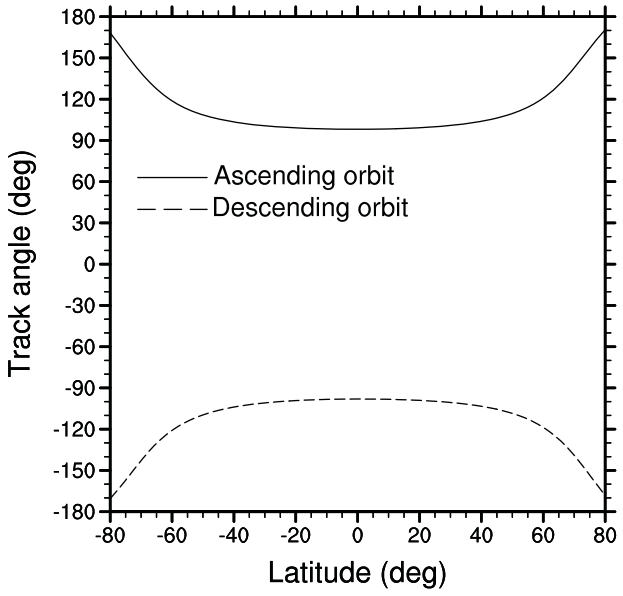

Figure 2. Track angles (α_T) as a function of latitude for ascending (solid line) and descending (dashed line) orbits.

appropriate conversion factor, which is the same as in the work of *Choi et al.* [2009] (i.e., $c_f = 375$). The horizontal wave number (k_h) is analytically calculated as $k_h(c,\varphi) = 2\pi/(\delta_h\sqrt{\pi})/\sqrt{1+\left[c-c_{qh}(\varphi)\right]^2/c_0^2}$, where $c_0 = \delta_h/\delta_t$ and c_{qh} is the moving speed of the convective source, which was updated recently by the basic state wind averaged below 700 hPa [*Choi and Chun*, 2011]. For a given forcing scales (i.e., $\delta_h = 5$ km and $\delta_t = 20$ min) and the phase speed range of -100 to 100 m s^{-1} at intervals of 2 m s^{-1}, the spectral peak of the GW momentum flux near cloud top occurs at horizontal wavelength $\lambda_h \sim 10$ km. However, the GW spectrum underestimates momentum flux in the AIRS-visible spectral portion ($\sim$40 km $< \lambda_Y <$ 500 km), which is addressed by including an additional cloud top GW momentum flux spectrum with longer horizontal wavelength components (see Figure 5). Details on the GW spectrum and parameters can be found in the work of *Song and Chun* [2005], *Song et al.* [2007], and *Choi and Chun* [2011].

[14] After the GW momentum flux and properties at cloud top are specified, second a trajectory of each GW packet is calculated by using a three-dimensional ray-tracing model [*Lighthill*, 1978]. The parameterization considers both the horizontal and vertical propagations of GW. For this reason, the waves can propagate beyond the grid box where they are originally launched. Finally, the deposition of GW momentum forcing into the ambient flow through critical level filtering, wave breaking, and wave diffusion processes is calculated on the basis of a Lindzen-type saturation method [*Lindzen*, 1981]. The calculation procedures for the parameterization are identical to those used in the work of *Choi et al.* [2009], except that the cloud top GW spectrum is recalculated on the basis of an update of c_{qh} in the work of *Choi and Chun* [2011].

[15] The convective heating for the offline calculation is obtained from the 6 hourly DCH of the National Centers for Environmental Prediction (NCEP) Department of Energy (DOE) reanalysis data 2 on T62 (192 $\times$ 94) quadratic Gaussian grids and 28 sigma levels ranging between 1000 and 2.5 hPa [*Kanamitsu et al.*, 2002]. Convective properties such as the cloud top and bottom are also estimated from the vertical profile of the DCH. As for the background atmosphere, the 6 hourly wind and temperature of the European Center for Medium-Range Weather Forecasts (ECMWF) ERA-Interim reanalysis on 1.5° $\times$ 1.5° grids and 37 pressure levels ranging from 1000 to 1 hPa are used [*Simmons et al.*, 2006]. A total of 101 GW packets in the phase speed range of -100 to 100 m s^{-1} with an interval of 2 m s^{-1} are launched in each azimuthal direction every 6 h at the cloud top.

[16] The GWTVs from the parameterization are calculated at $z = 2.5$ hPa (unfiltered GWTV), after which AIRS-filtered GWTVs to be compared directly with the AIRS measurements are calculated by applying the 2-D AIRS visibility function of Figure 1a to the unfiltered GWTVs. To apply the AIRS visibility function to GW packets as in the work of *McLandress et al.* [2000] and *Jiang et al.* [2004a] for the MLS observations, we compute the cross-track (k_Y) and vertical (k_Z) wave numbers for each GW packet with wave numbers (k, l, m) in the usual x-y-z coordinate system as follows:

$$\begin{aligned} k_Y &= K_h \sin(\varphi - \alpha_T) = -k\sin\alpha_T + l\cos\alpha_T, \\ k_Z &= m, \end{aligned} \tag{1}$$

where α_T is the track angle measured counterclockwise from the east to the axis along the satellite's moving direction (Figure 2). The parameterized AIRS-filtered GWTVs are averaged for ascending and descending orbits because there are no significant differences between the two. The GWTVs from the CGWD parameterization are primarily compared with the AIRS GWTVs averaged across entire view angles. In addition, the eastward and westward GWTVs calculated from the parameterization are separately compared with the AIRS GWTVs observed at the west and east views, respectively. Note again that in the west (east) FOV of AIRS, eastward (westward) propagating GWs are favorably detected.

3. Results

3.1. Comparison Between CGWD Parameterization Calculations and AIRS Observations

[17] Figure 3 shows the AIRS GWTVs, as well as the unfiltered and AIRS-filtered GWTVs calculated from the parameterization (without the additional GW spectrum) at $z = 2.5$ hPa for January and July 2005, together with the maximum NCEP DCH in the troposphere as an indicator for deep convections. Although AIRS samples each 2° $\times$ 2° latitude-longitude grid box, the AIRS GWTVs in this study are regridded onto 10° $\times$ 5° boxes for better visualization, as are the GWTVs from the parameterization. The GWTV map is displayed only for the tropics and subtropics where convective sources are strong, because we are interested in the convectively induced GWs. The NCEP DCH shows deep convections in the tropical and summer subtropical regions. The AIRS GWTVs in the summer subtropics in both January and July correlate well with the strong NCEP DCH in the same regions, indicating that the

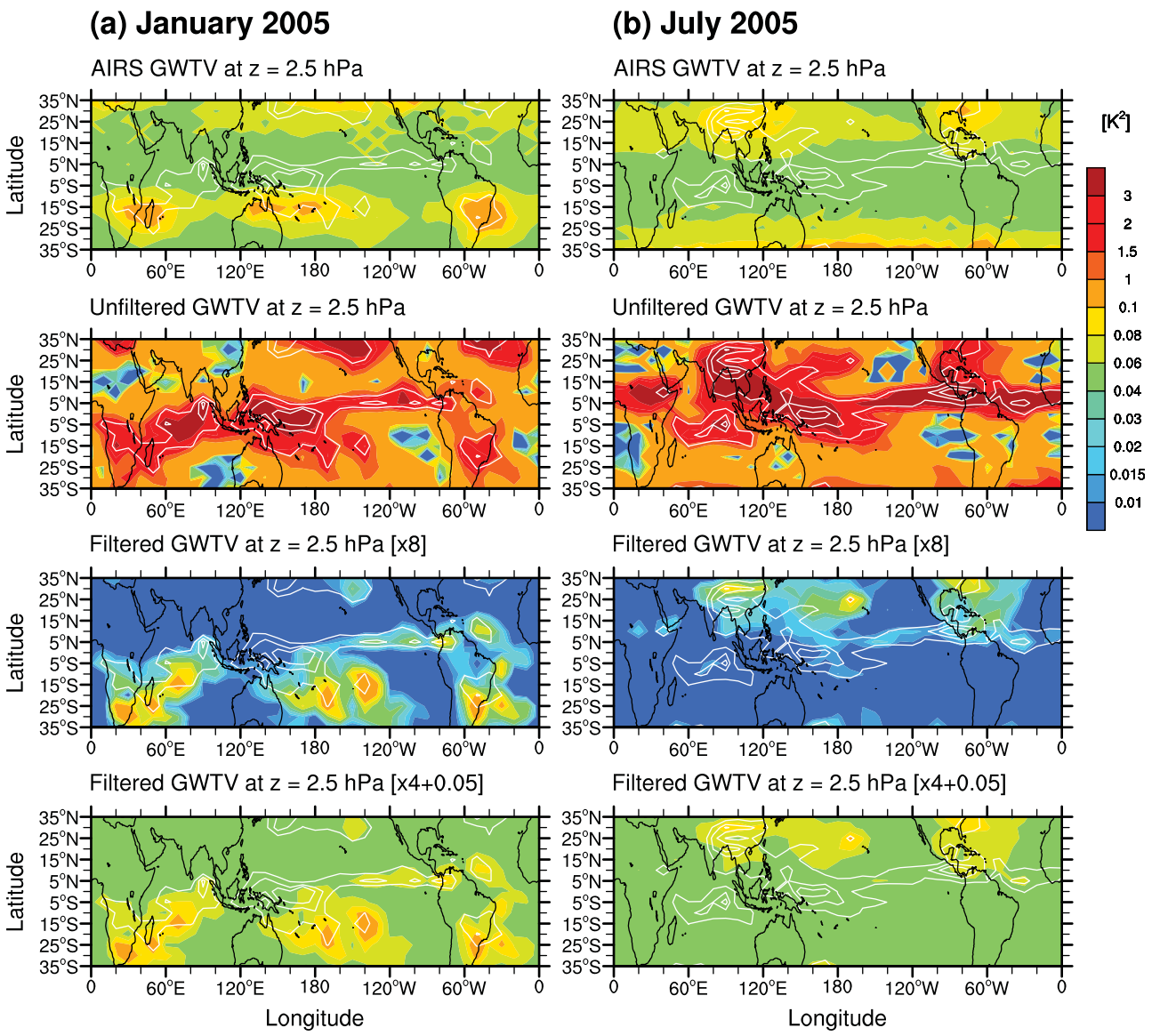

Figure 3. AIRS GWTVs, as well as unfiltered GWTVs and AIRS-filtered GWTVs without and with the correction by adding the background variance (0.05 K^2) from the parameterization at z = 2.5 hPa for (a) January and (b) July 2005. White lines denote the contours of the maximum NCEP DCH with 5, 8, and 10 K d^{-1} in the troposphere. The AIRS-filtered GWTVs from the parameterization without and with the correction by the background variance are multiplied by factors of 8 and 4, respectively.

observed GW activities are induced by convective GWs. However, GWTVs are nearly absent in the equatorial regions (10°S–10°N) despite strong tropical convections. The reason is revealed by the following parameterization results. The unfiltered GWTVs from the parameterization exhibit peaks above strong convective clouds in equatorial regions (10°S–10°N) with a magnitude of ~3 K^2 or more. They differ considerably from AIRS GWTVs that peak in the summer subtropics (10°S–30°S in January; 15°N–35°N in July). The amplitude of the parameterized GWTV is about 30 times larger than that of the AIRS GWTV. However, the amplitude of unfiltered GWTVs in the equatorial regions is substantially attenuated by applying the AIRS visibility function, and the spatial distribution of AIRS-filtered GWTVs correlates well with that of AIRS GWTVs with peaks in the summer subtropics for both January and July 2005.

[18] To understand the differences between the unfiltered and AIRS-filtered GWTVs from the parameterization, in Figure 4 we display their spectral distributions in the summer subtropics (at 20°S) and tropics (at the equator) at z = 2.5 hPa for January 2005, along with the 2-D AIRS visibility. As in Figure 3, the unfiltered GWTVs from the parameterization are stronger at the equator than in the summer subtropics. This is because convective sources are stronger at the equator and the parameterized GWTVs at the source level are larger at the equator than in the subtropics. However, most GWTVs at the equator are within the spectral ranges of short horizontal and vertical wavelengths where AIRS GW visibilities are weak; thus, they are mostly

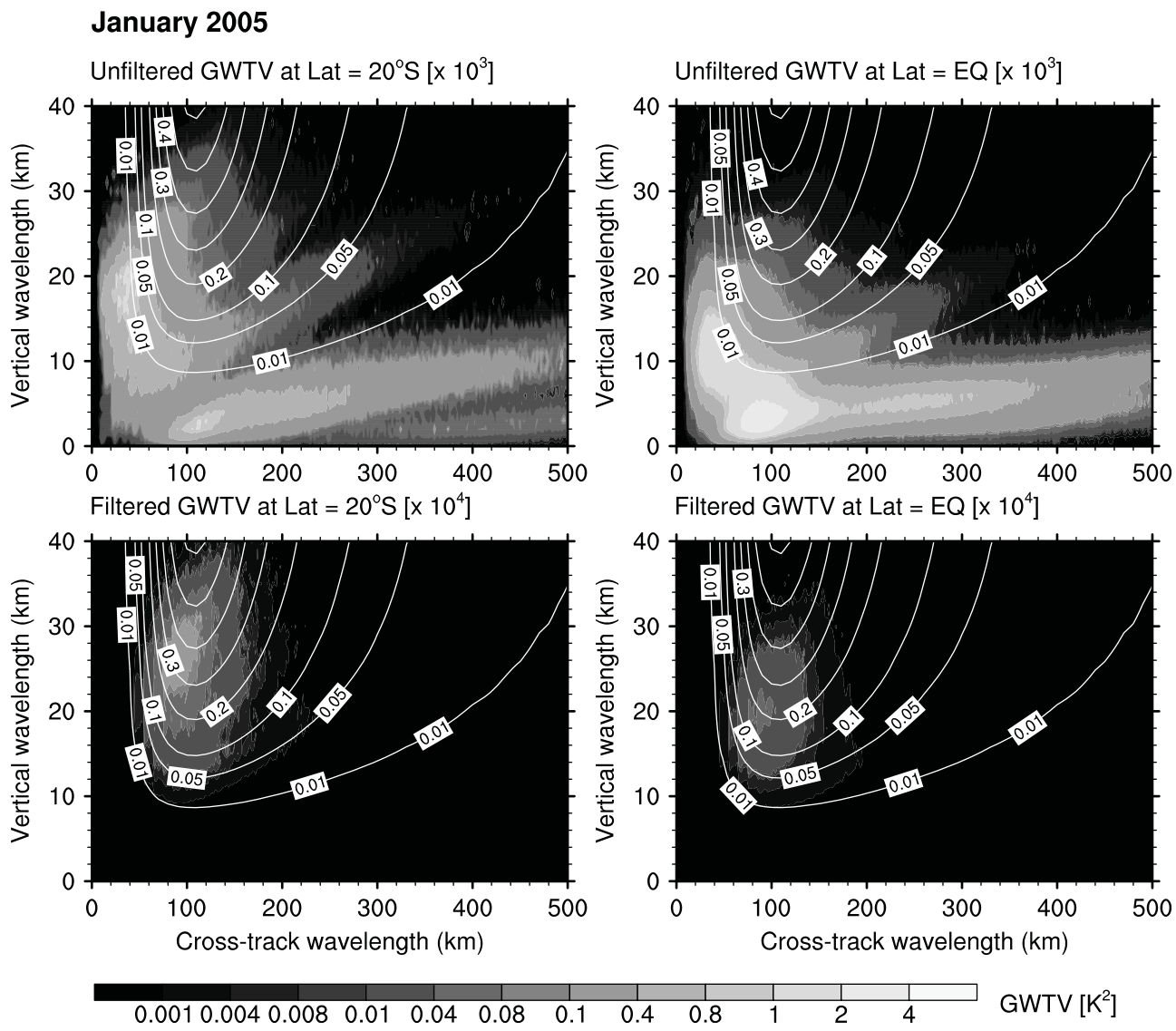

Figure 4. Unfiltered and AIRS-filtered summer subtropical (at 20°S) and tropical (at equator) GWTVs at z = 2.5 hPa from the parameterization for January 2005 (shading) and the 2-D AIRS visibility (white lines) as a function of the cross-track and vertical wavelengths. The unfiltered and AIRS-filtered GWTVs are multiplied by factors of 10^3 and 10^4, respectively.

filtered out when the AIRS GW visibility function is applied. The GWTVs in the spectral ranges with large AIRS GW visibilities (i.e., with long vertical wavelengths) are stronger in the summer subtropics than in the tropical regions; thus, the AIRS-filtered GWTVs are more noticeable in the summer subtropics than at the equator. The contrast between the tropics and subtropics is likely due to the difference in the upper stratospheric winds. Although the horizontal and vertical scales of GWs at the source level are not significantly different between the two regions except for the larger GW magnitude in the tropics, upper stratospheric winds are stronger in the subtropics than in the tropics, and GWs are expected to be refracted more toward longer vertical wavelengths in the upper stratospheric subtropics. Therefore, GWs in the summer subtropics of the upper stratosphere are more visible to AIRS than are those in the tropics. This is the main reason that AIRS GWTVs are dominant in the summer subtropics at z = 2.5 hPa despite the stronger convective GW sources in the tropics. The lack of stratospheric tropical (10°S–10°N) GWs in the observations is discussed further in section 3.2.

[19] Although the spatial distribution of AIRS GWTVs can be reproduced by the parameterization, the magnitude of the AIRS-filtered GWTVs is still much too small compared to the observations (~8 times smaller, as shown in Figure 3; note that the AIRS-filtered GWTVs are multiplied by a scaling factor of 8). This is likely because the AIRS measurements include other signals besides the convective GWs. The AIRS measurements show a uniform background-like variance with a magnitude of ~0.05 K^2, which is not closely correlated with deep convections, even in the winter subtropical continents. The background-like variance was not found in the tropics and subtropics of the UARS MLS observations [*Jiang et al.*, 2004b; *Choi et al.*, 2009]. Therefore, we assume that this variance is due to signals other than convective GWs. *Gong et al.* [2011] provided a

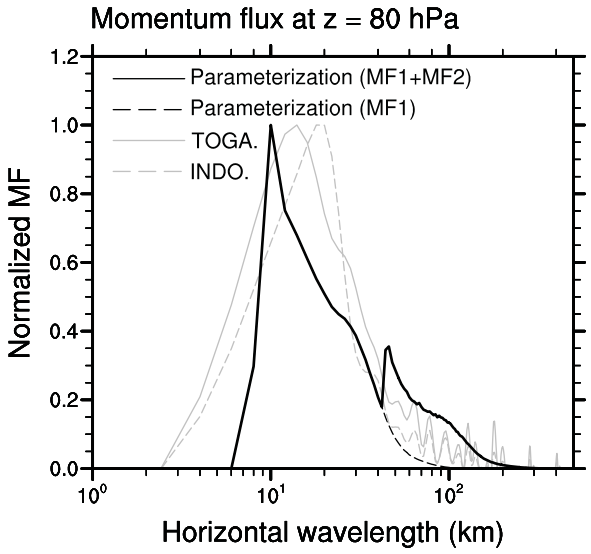

Figure 5. GW momentum flux at z = 80 hPa as a function of horizontal wavelength from the parameterization with both primary and secondary GW spectra (MF1+MF2, black solid line) and with the primary GW spectrum (MF1, black dashed line) for January 2005 and from the mesoscale simulations for the Tropical Ocean Global Atmosphere Coupled Ocean-Atmosphere Response Experiment (TOGA., gray solid line) and Indonesia (INDO., gray dashed line) cases performed in the work of *Choi and Chun* [2011]. The momentum flux for each spectrum is normalized by its maximum magnitude.

careful evaluation of noise of the AIRS observations and, on the basis of Gong et al., the background variance is unlikely to be a pure noise. The possible sources of the background variance include some low-frequency inertial GWs with long horizontal and short vertical wavelengths, which were shown to contribute significantly to the AIRS variances [*Gong et al.*, 2011, section 4.3]. Because the convective GWs parameterized in the present study are the sub-grid-scale internal GWs, addition of the background variance that largely represents inertial GWs is required in order for direct comparison with the AIRS observations. On the basis of this, the AIRS-filtered GWTVs from the parameterization are corrected by adding the background variance (0.05 K^2), and then displayed in Figure 3. The corrected AIRS-filtered GWTVs correlate better with the AIRS GWTVs. However, the magnitude is still about four times smaller than the AIRS measurements. This indicates that the parameterization probably underestimates the momentum flux of convective GWs in the spectral portions visible to AIRS ($\sim$40 km < λ_Y < 500 km and λ_Z > 12 km).

[20] To check this possibility, we compare the spectral distribution of the GW momentum flux from the parameterization with distributions from the mesoscale simulations carried out for two tropical storm cases in the work of *Choi and Chun* [2011]. One is the Tropical Ocean Global Atmosphere Coupled Ocean-Atmosphere Response Experiment (TOGA COARE) case reported by *Trier et al.* [1996]; the other is the Indonesia case reported by *Dhaka et al.* [2005]. Figure 5 shows the spectral distributions of the GW momentum flux near the source level (at z = 80 hPa) with respect to the horizontal wavelength (λ_h) from the offline calculation of the parameterization for January 2005 and from the mesoscale simulations for the TOGA COARE and Indonesia cases. The spectral peak of the GW momentum flux from the parameterization occurs near λ_h = 10 km, which roughly matches the λ_h values for the primary peaks of GW spectra from the mesoscale simulations. However, it is found that the parameterization severely underestimates the GW momentum flux at λ_h > $\sim$40 km, which is a range in which GWs are visible to AIRS. Because critical level filtering of GWs by the background atmosphere from the cloud top to 80 hPa is not significant, the differences between the parameterization and mesoscale simulation results are unlikely owing to the different GW filtering between the parameterization and mesoscale simulations.

[21] To overcome this limitation, a secondary GW spectrum (MF2) is included in the parameterization in addition to the original primary GW spectrum (MF1). The MF2 is calculated using the same formulas for the GW spectrum and convective source spectrum as those for the MF1, except for the larger spatial and temporal scales of the diabatic forcing (δ_h = 25 km and δ_t = 60 min for MF2, δ_h = 5 km and δ_t = 20 min for MF1) and hence the strong GW momentum flux at λ_h > $\sim$40 km with a spectral peak at a longer horizontal wavelength ($\sim$50 km) than the primary spectral peak ($\sim$10 km). The phase-speed range and the wave propagation directions are also the same as those for the MF1; thus, the number of launched rays is also the same. The magnitude of the convective source, which determines the magnitude of the GW momentum flux, is assumed to be 15 times smaller than that for the primary GW spectrum on the basis of the simulation results (see *Choi and Chun* [2011, equations (1) and (2)] for the GW spectrum and convective source spectrum). The GW momentum flux spectrum from the parameterization with both MF1 and MF2 is displayed in Figure 5. When both MF1 and MF2 are considered, the GW spectrum from the parameterization is more closely correlated with the GW spectra from the mesoscale simulations.

[22] Subsequently, the GWTVs are recalculated from the parameterization with both the primary and secondary GW spectra. Figure 6 shows the AIRS GWTVs and AIRS-filtered GWTVs from the parameterizations with only the primary GW spectrum (MF1) and with both the primary and secondary GW spectra (MF1+MF2) at z = 2.5 hPa for January and July 2005. The GWTVs from the parameterization are corrected by adding the background variance (0.05 K^2) shown in the AIRS measurements. The spatial distributions of AIRS-filtered GWTVs from both parameterizations with MF1 and MF1+MF2 agree well with those of AIRS GWTVs with peaks in the summer subtropics. However, the magnitude of the GWTVs by MF1 alone is about four times smaller than that of AIRS. The magnitude increases by including the MF2 in addition to the MF1. Furthermore, both the magnitude and spatial distribution of the AIRS-filtered GWTVs from the parameterization with MF1+MF2 are in good agreement with the AIRS observations. Besides, the parameterization with MF1+MF2 simulates the reasonable vertical wave number (m) spectrum of GW energy, of which a shape well matches with that of GW spectrum found from GW measurements (i.e., $\propto m^{-3}$ at large m) [see *Fritts and Chou*, 1987] and so does the parameterization with MF1 only (Figure 7).

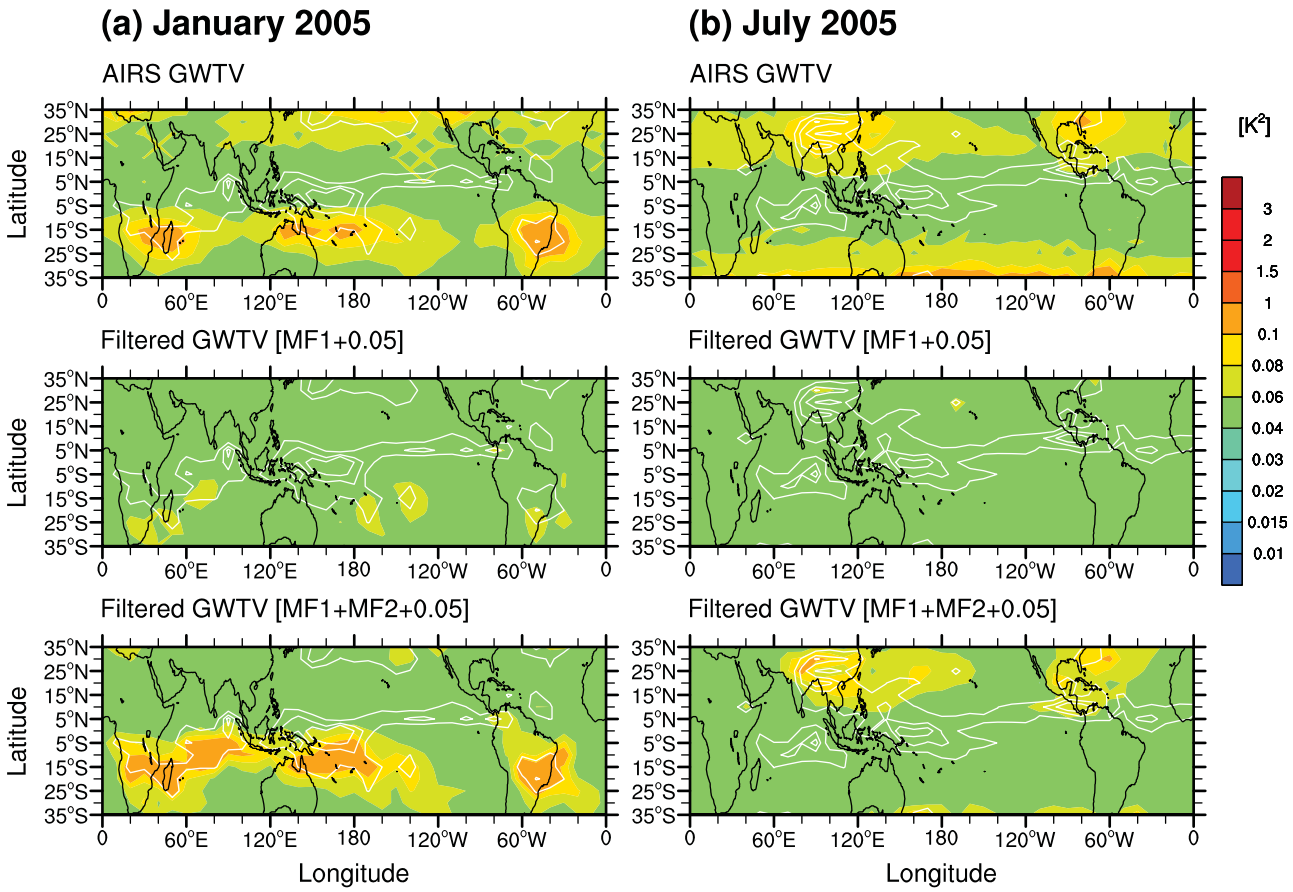

Figure 6. AIRS GWTVs and AIRS-filtered GWTVs from the parameterizations with the primary GW spectrum (MF1) and with both primary and secondary GW spectra (MF1+MF2) corrected by adding the background variance (0.05 K^2) at z = 2.5 hPa for (a) January and (b) July 2005. White lines denote the contours of the maximum NCEP DCH with 5, 8, and 10 K d^{-1} in the troposphere.

[23] Although the parameterization with the primary spectrum (MF1) could represent the GW variances observed by UARS MLS reasonably well in the work of *Choi et al.* [2009], the addition of the secondary spectrum is likely better for representing GWs observed in such sublimb sounders as well.

[24] The parameterization results (MF1+MF2) in Figure 6 show some disagreements with the AIRS observations in several regions. In the winter subtropics of 25°N–35°N for January and 25°S–35°S for July, the GWTVs from the parameterization are much smaller than the observed GWTVs. The GWs in these regions are likely to be generated by other sources such as jet front systems, frontogenesis [*Richter et al.*, 2010], and topography [*Jiang et al.*, 2004a, 2004b] in addition to convective sources. A similar disagreement found in the northern summer subtropics can be explained by the same reason. *Jiang et al.* [2004b] showed that stratospheric (at 5 hPa) mountain waves can be found over northeast Africa, the Middle East, northern India, and Mexico even during northern summers, although deep convection is the major source of the strong stratospheric GWs in the northern summer subtropics. This indicates that the AIRS measurements in the present northern summer subtropics might include mountain GWs as well as convective GWs. In the southern summer subtropics, the topography-

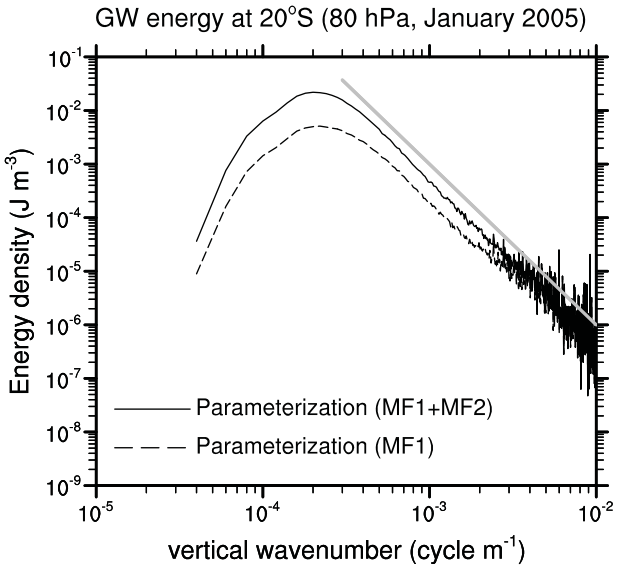

Figure 7. GW energy as a function of vertical wave number in the summer subtropics (20°S) at z = 80 hPa from the parameterizations with MF1 only (black dashed line) and with both MF1 and MF2 (black solid line) for January 2005. The thick gray line represents the slope of m^{-3}.

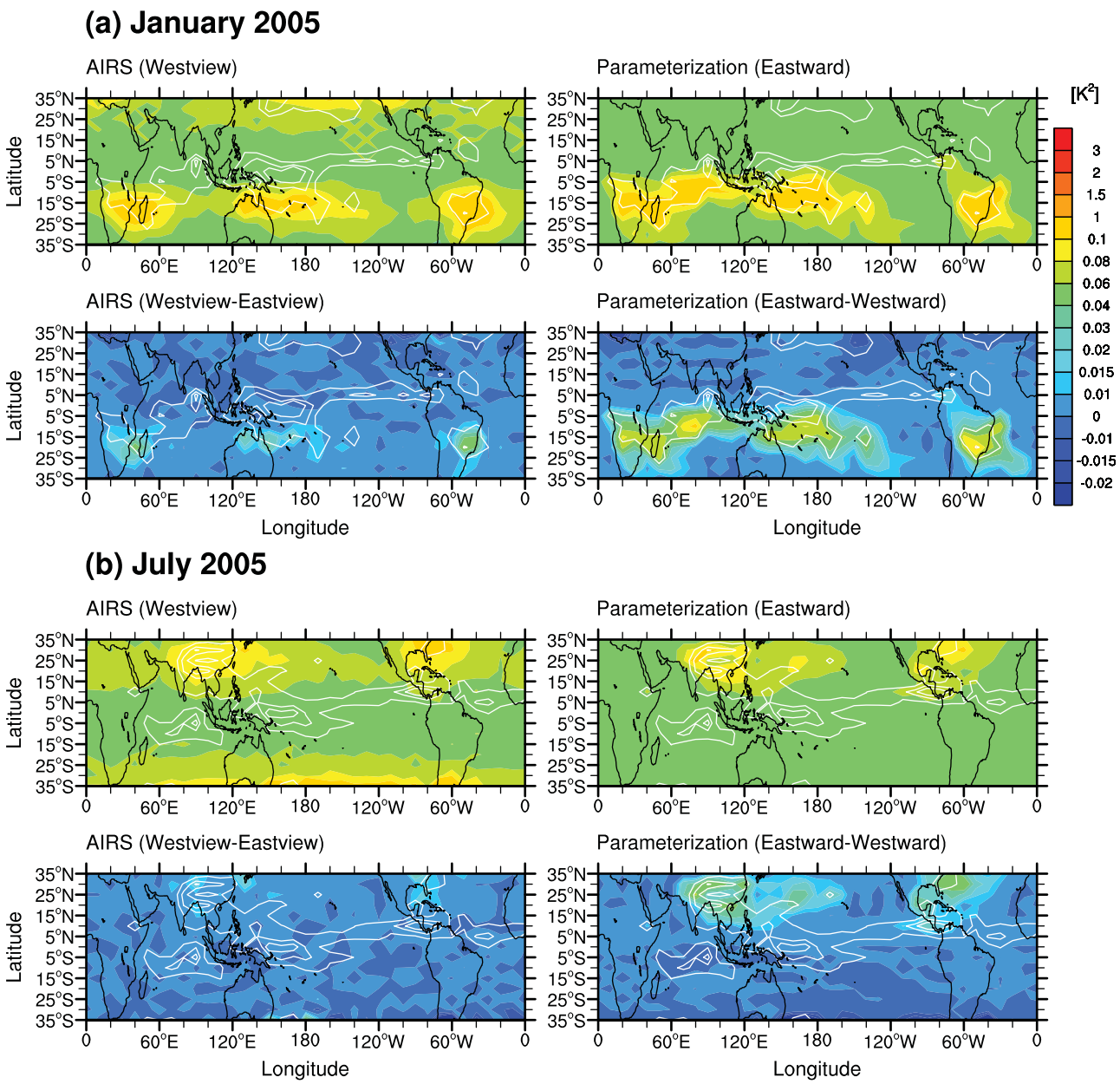

Figure 8. AIRS GWTVs from a west view, the differences between the GWTVs at west and east views (Westview-Eastview), the AIRS-filtered eastward GWTVs from the parameterization with both MF1 and MF2 corrected by adding the background variance, and the differences between the AIRS-filtered eastward and westward GWTVs (Eastward-Westward) for (a) January and (b) July 2005.

related GW activities in the stratosphere are unlikely to be significant [see *Jiang et al.*, 2004b, Figure 9], and the match between the parameterized convective GWTVs and observations is better in the southern summer subtropics than in the northern summer subtropics. The disagreement between the parameterization and the AIRS observations may be also due to some assumptions used in the current CGWD parameterization, such as the neglect of horizontal refraction, time invariant ground-based frequency, and 1 day lifetime of rays.

[25] AIRS favorably detects the eastward (westward) GWs in the west (east) FOVs of AIRS. Thus, the preferred zonal GW propagation direction can be inferred by the difference between the GWTVs of the west and east views [*Gong et al.*, 2011]. In this study, eastward and westward components of the AIRS-filtered GWTVs from the parameterization are also computed at $z = 2.5$ hPa for January and July 2005 and compared with the AIRS GWTVs at the west (averaged for $-48.95°$ and $0°$) and east (averaged for $0°$ and $48.95°$) views, respectively (Figure 8). The GWTVs from the parameterization are calculated using both MF1 and MF2 and corrected by adding the background variance of the AIRS GWTVs. The distributions of the AIRS GWTVs at the west and east views (not shown) are similar with peaks in the summer subtropics, although the magnitude is larger for the west-view observations (see Westview-Eastview of

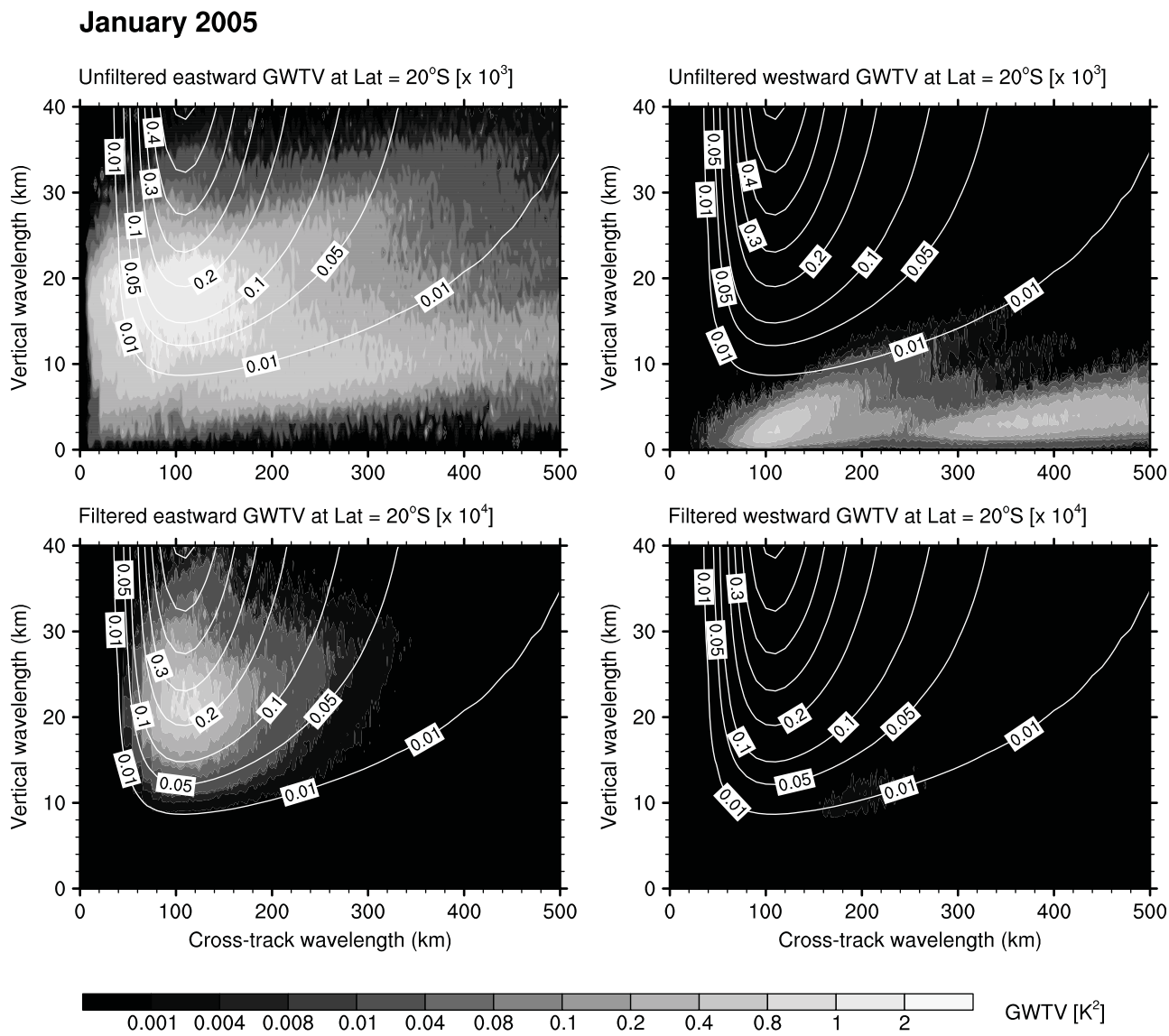

Figure 9. Unfiltered and AIRS-filtered summer subtropical (at 20°S) eastward and westward GWTVs at z = 2.5 hPa from the parameterization (shading) and the 2-D AIRS visibility (white lines) as a function of the cross-track and vertical wavelengths for January 2005. The unfiltered and AIRS-filtered GWTVs are multiplied by factors of 10^3 and 10^4, respectively.

Figure 8). This indicates that the eastward components of convective GWs in the summer subtropical upper stratosphere are predominantly observed by AIRS, implying that the convective GWs in this region mostly propagate eastward. Consistent with the result in the AIRS observations, the parameterization calculation shows that the AIRS-filtered eastward GWTVs are larger than the westward GWTVs (see eastward-westward). However, the difference between the eastward and westward GWTVs from the parameterization is larger than that between the west view and east view observations. This is mainly because the west view (east view) observations are not perfect observations of the eastward (westward) propagating GWs with the perfect filter of westward (eastward) propagating GWs. For this reason, the GWTVs observed in the AIRS west view (east view) cannot be compared directly with the eastward (westward) GWTVs from the parameterization in terms of the magnitude. Only the prevailing zonal GW propagation direction can be inferred.

[26] To understand the difference between the eastward and westward GWTVs, we examine the spectral distributions of both components from the parameterization. Figure 9 shows the unfiltered and AIRS-filtered eastward and westward GWTVs at z = 2.5 hPa from the parameterization in the summer subtropics (at 20°S) where the GWTV peaks occur, and the 2-D AIRS visibility with respect to the cross-track and vertical wavelengths for January 2005. The spectra reveal very different distributions with few overlapped components between the two propagations. For the unfiltered GWTVs, the eastward GWTVs are generally stronger than the westward GWTVs. This is because some westward propagating GWs are filtered out by easterly winds in the summer subtropical stratosphere. There are no significant differences between the two components at the

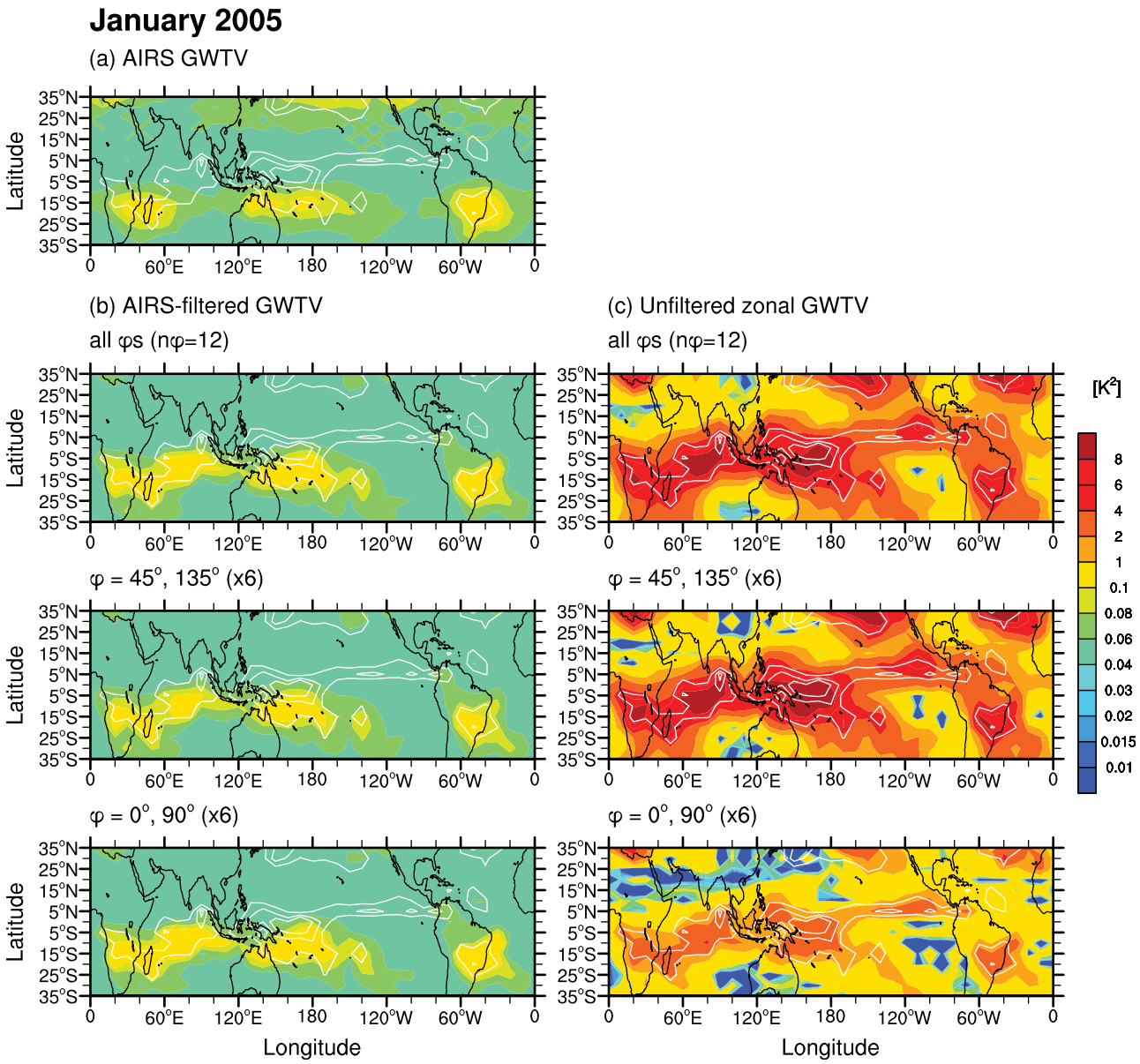

Figure 10. (a) AIRS GWTVs, (b) AIRS-filtered GWTVs, and (c) unfiltered zonal GWTVs from the parameterizations that consider (1) multiple wave propagation directions and two wave propagation directions of (2) 45° and 135° and (3) 0° and 90° at $z = 2.5$ hPa for January 2005. White lines denote contours of the maximum NCEP DCH with 5, 8, and 10 K d^{-1} in the troposphere. The AIRS-filtered GWTVs are calculated from the parameterization with both MF1 and MF2 and are corrected by adding the background variance of AIRS GWTVs. The AIRS-filtered and unfiltered GWTVs from the parameterizations with (2) and (3) are multiplied by a factor of 6 to assure a reasonable comparison with those obtained from the parameterization that considers multiple directions.

source level (not shown). The unfiltered eastward GWTVs are much stronger than the westward GWTVs, especially for long vertical wavelength components that are well visible to AIRS. This is because GWs propagating in the direction opposite to the subtropical easterly winds (i.e., eastward propagating GWs) are refracted to longer vertical wavelengths according to the dispersion relationship, $\lambda_z \propto |c - U|/N$, where c is the phase speed, U is the basic state wind, and N is the basic state Brunt-Väisälä frequency. However, westward propagating GWs are Doppler shifted toward shorter vertical wavelengths and become almost invisible to AIRS. Consequently, the eastward propagating GWs are preferentially observed by AIRS because of the critical level filtering of the westward propagating GWs and the refraction of the eastward propagating GWs to longer vertical wavelengths.

3.2. Sensitivity to the Wave Propagation Direction

[27] Although the CGWD parameterization can reproduce the observed AIRS GWTVs with multiple wave propagation directions, it is meaningful to check whether the parameterization can also reproduce the observed GWs by considering only the minimum number of wave propagation directions,

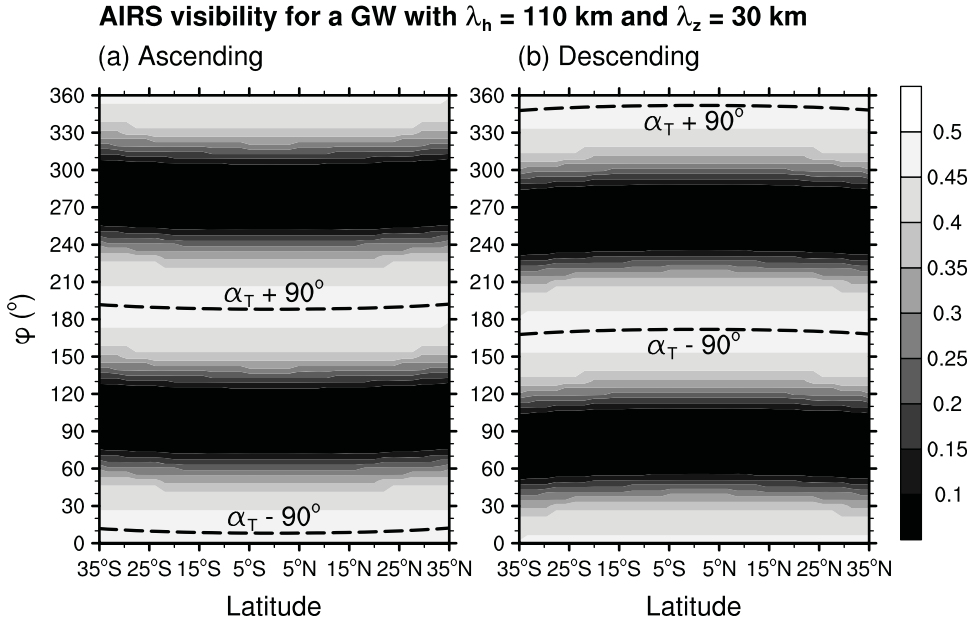

Figure 11. AIRS visibility for a monochromatic GW packet with a horizontal wavelength of 110 km and a vertical wavelength of 30 km as a function of latitude and wave propagation direction for (a) ascending and (b) descending orbits, respectively. Angles ($\alpha_T \pm 90°$) for the two propagation directions cross the track angle (α_T) are overplotted with black dashed lines.

an assumption generally adopted in the CGWD parameterization for computational efficiency. In this section, we investigate the sensitivity of the realism of the parameterization results to the choice of wave propagation direction.

[28] Figure 10 displays the AIRS GWTVs, and AIRS-filtered GWTVs and unfiltered zonal GWTVs from the parameterization with three different choices of wave propagation direction (φ = (1) 15°n, n = 0, 1,…, 11, (2) 45° and 135°, and (3) 0° and 90°) at z = 2.5 hPa for January 2005. The maximum NCEP DCHs for January and July 2005 are overplotted in Figure 10. The wave propagation directions of 45° (northeast-southwest) and 135° (northwest-southeast) were selected as the best directional pair for computational efficiency in the work of *Choi and Chun* [2011], and the directions of 0° (east-west) and 90° (north-south) were used in the original parameterization [*Song and Chun*, 2008]. The AIRS-filtered GWTVs are calculated from the parameterization with both MF1 and MF2 and corrected by adding the background variance of AIRS GWTVs. The AIRS-filtered GWTVs from the parameterizations with (2) and (3) are multiplied by a factor of 6 to assure a reasonable comparison with that obtained from the parameterization that considers multiple directions. Comparisons among the results from the parameterizations with the three different choices and the AIRS measurements reveal that the AIRS-filtered GWTVs from the parameterization with the two directions of (2) or (3) agree well not only with those from the parameterization using multiple directions, but also with the AIRS GWTVs. This indicates that the parameterization can reproduce the AIRS GWTVs realistically with only the minimum number of wave propagation directions. When the directional pair of (2) is considered, GWs in both directions of 45° and 135° contribute to the AIRS-filtered GWTVs from the parameterization. However, when the directional pair of (3) is considered, only the GWs in the direction of 0° contribute to the AIRS-filtered GWTVs from the parameterization.

[29] The sensitivity of the AIRS-filtered GWTV to the wave propagation direction is largely due to that of the AIRS visibility to the wave propagation direction. Figure 11 shows the AIRS visibility for a monochromatic GW packet with a horizontal wavelength of 110 km, near which the maximum AIRS cross-track visibility occurs, and a vertical wavelength of 30 km plotted on a two-dimensional grid of latitude and wave propagation direction for ascending and descending orbits, respectively. The intrinsic phase speed of the GW packet shown in Figure 11 is about 100 m s^{-1}, and it is not unrealistic for the convective gravity waves [see *Alexander et al.*, 2010, Figure 8]. Although the cloud top momentum flux of GWs with phase speeds larger than about 60 m s^{-1} are not significant in their magnitudes [see *Song et al.*, 2007, Figure 1], those GWs are very important because they are the ones to propagate into the upper mesosphere without the critical level filtering and to deposit large amount of momentum there when they are dissipated. The visibility with respect to wave propagation direction shows that the AIRS visibility is strong near the wave propagation directions parallel to the cross-track directions (i.e., $\alpha_T \pm 90$). This indicates that the GW components lying along the cross-track direction are favored by AIRS. The AIRS visibility is strong for the GWs propagating near the zonal direction (φ = 0° and 180°) because the orbital tracks of the AIRS observations are primarily in the meridional direction. The AIRS visibility decreases as the wave propagation direction rotates away from the zonal direction, and the minimum AIRS visibility occurs near the meridional direction (φ = 90° and 270°). Therefore, only GWs in the direction of 0° with strong AIRS visibility contribute to the AIRS-filtered GWTVs from the parameterization with the

wave propagation directions of 0° and 90°. Note that the φ in this study, except in Figure 11, includes both φ and φ +180°.

[30] Although the AIRS GWTVs are reproduced by both parameterizations with the two wave propagation directions of (2) 45° and 135°, and (3) 0° and 90°, the unfiltered GWTVs from multiple directions of the full spectral range without observational filtering are reproduced only when the directional pair of 45° and 135° is chosen (see Figure 10c for the unfiltered zonal GWTV). The parameterization with φ = 0° and 90° underestimates the unfiltered zonal GWTVs compared to those from multiple wave propagation directions. The meridional GWTVs as well as the zonal GWTVs are underestimated; this implies that both zonal and meridional GW components integrated over a full spectral range may be underestimated in the parameterization when the directional pair of 0° and 90° is chosen. This result is consistent with that in the work of *Choi and Chun* [2011]. Consequently, it is found that the parameterization with the wave propagation directions of 45° and 135° can reproduce not only AIRS-observable GWs but also GWs from multiple directions of the full spectral range. However, the parameterization with the directions of 0° and 90° can reproduce GWs of the AIRS-visible spectral portion but cannot reproduce GWs from multiple directions of the full spectral portion.

4. Summary and Discussion

[31] In this study, the realism of the ray-based CGWD parameterization is tested through comparisons with the AIRS observations of GW activity in the upper stratosphere. The AIRS observations detect GWs with a relatively high frequency and short horizontal wavelength. Thus, they are appropriate for the validation of convective GWs parameterized with short horizontal wavelengths.

[32] To validate the parameterization, AIRS GWTVs at z = 2.5 hPa with clearly observable GW signals associated with deep convections for January and July 2005 are used. The mean values of AIRS GWTVs from the ascending and descending orbits averaged for view angles of $\pm$ 48.95° are used, and the AIRS observations at the west and east FOVs are also separately compared with the eastward and westward GW components, respectively, from the parameterization. In the west (east) FOV of AIRS, the eastward (westward) GWs are detected favorably.

[33] The CGWD parameterization uses the moving speed of the convective source updated in the work of *Choi and Chun* [2011] and considers multiple wave propagation directions (φ = 15°n, n = 0, 1,…, 11) for more realistic GW effects. Offline calculation of the ray-based CGWD parameterization is carried out with the ECMWF ERA-Interim reanalysis data for the background atmosphere and the NCEP DOE reanalysis 2 data for the DCH as the convective source for January and July 2005. The GWTVs from the parameterization are calculated at z = 2.5 hPa (unfiltered GWTVs), and the unfiltered GWTVs are filtered by the 2-D AIRS visibility function (AIRS-filtered GWTVs) for a direct comparison with the AIRS observations. The AIRS-filtered GWTVs from the parameterization are corrected by the background-like variance ($\sim$0.05 K^2) included in the AIRS GWTVs, which is likely to be associated with inertial GWs rather than convective GWs. The parameterization results are compared with the AIRS observations only in the tropics and subtropics where the deep convection is the major source of GWs.

[34] The comparison between the parameterization results and AIRS observations can be summarized as follows: (1) the unfiltered GWTVs from the parameterization are much larger than the AIRS GWTVs and their peaks occur in the tropics, collocating with strong convective activities; (2) the magnitude of the unfiltered GWTVs is significantly reduced by applying the AIRS visibility function, and the spatial distribution of the AIRS-filtered GWTVs agrees well with that of AIRS GWTVs with peaks in the summer subtropics; and (3) the magnitude of the AIRS-filtered GWTVs from the parameterization is smaller than that of the AIRS GWTVs because the GW momentum flux in the AIRS-visible spectral portion ($\sim$40 km < λ_Y < 500 km and λ_Z > 12 km) is underestimated in the parameterization. When an additional GW momentum flux spectrum (MF2) with longer horizontal and vertical wavelengths is included in the parameterization, both the magnitude and spatial distribution of the AIRS-filtered GWTVs from the parameterization are in good agreement with those of the AIRS GWTVs.

[35] The eastward and westward AIRS-filtered GWTVs from the parameterization are separately compared with the AIRS GWTVs at the west and east FOVs, respectively. In the parameterization calculation, the AIRS-filtered eastward GWTVs are larger than the westward GWTVs, which is consistent with the stronger GW activities at west-viewing AIRS observations. The stronger eastward GW activities in both the parameterization results and AIRS observations are due to the filtering out of some westward propagating GWs by easterly winds in the summer subtropical upper stratosphere. Another reason is that GWs propagating in the direction opposite to the winds (i.e., eastward propagating GWs) are Doppler shifted toward longer vertical wavelengths and become more visible to AIRS.

[36] The sensitivity of the AIRS-filtered GWTVs from the parameterization to the wave propagation direction is investigated. Three different choices of wave propagation direction are considered ((1) multiple directions, (2) 45° (northeast-southwest) and 135° (northeast-southwest), and (3) 0° (east-west) and 90° (north-south)). The directional pairs of (2) and (3) are those chosen in previous studies (see *Choi and Chun* [2011] and *Song and Chun* [2008], respectively). Given that the minimum number of wave propagation directions is chosen in the parameterization for computational efficiency, it is important to verify whether the parameterization with (2) or (3) can reproduce the observed GW activities. The results of the sensitivity test show that the parameterization with (2) or (3) can reproduce the AIRS observable GWs. However, the unfiltered GWTVs from multiple directions integrated over a full spectral portion are reproduced only by the parameterization with (2). The parameterization with (3) substantially underestimates the unfiltered GWTVs. This is consistent with the result of *Choi and Chun* [2011], which showed that 45° and 135° is the best directional pair when two wave propagation directions are required in the parameterization for computational efficiency.

[37] In the present study, the realism of the CGWD parameterization is validated against the AIRS GW observations, and the parameterization is improved on the basis of

the observations. The AIRS measurements observe GWs in a tail portion of the convective GW spectrum and provide information for constraining GWs of the spectral portion in the parameterization. In order to reproduce the AIRS GW observations, a secondary GW spectrum that corresponds to the long horizontal wavelength tail of the spectrum from the mesoscale simulation results by *Choi and Chun* [2011] is added to the parameterization. The improved parameterization represents the GW variance observed by AIRS reasonably well.

[38] However, the comparisons between the parameterization calculations and the AIRS observations are limited only in the portion of the GW spectrum visible to AIRS; thus, realism of the parameterized convective GWs with a smaller scale invisible to AIRS is required to test against other observations with higher resolution. Although GW parameterizations are constrained by the multiple satellite measurements, there still exists a gap in the GW spectrum not covered by the existing satellite instruments. The gap would be able to be partially covered by other measurements such as superpressure balloons [*Alexander et al.*, 2010]. However, new instruments with better resolution are still required to fully constrain the parameterized GW spectrum. In particular, our unfiltered parameterization result shows strong activities of the convective GWs with small horizontal and vertical scales in the tropical regions (10°S–10°N), but the tropical GWs are rarely observed by AIRS owing to its coarse vertical resolution. The lack of stratospheric tropical GWs is also found from some sublimb sounder measurements (e.g., *Jiang et al.* [2004b] and *Choi et al.* [2009] from UARS MLS; *Wu and Eckermann* [2008] from Aura MLS). *Choi et al.* [2009] applied the observational filter of UARS MLS to parameterized GWs and found that the lack of tropical GWs is mainly due to that the tropical GWs with smaller vertical scales than the subtropical GWs are invisible to the instrument. Contrary, noticeable GW variances (or amplitude) are found in the tropics as well as in the subtropics from some IR limb sounder observations with higher vertical resolution than the sublimb and nadir sounders (e.g., *Ern et al.* [2004, Figure 3b] for CRISTA; *Preusse et al.* [2009, Figure 5] for SABER; and *Wang and Alexander* [2010, Figure 3] for GPS) except for HIRDLS [*Yan et al.*, 2010, Figure 5; *Wright and Gille*, 2011]. The HIRDLS observations show relatively weak equatorial GW activities in spite of the highest vertical resolution (~1 km) compared with the aforementioned limb sounders. This implies that the observational filter largely depends on the geometry of satellite motion (e.g., track angle) as well as the resolution of the instrument.

[39] The parameterization results in this study show some disagreements with the AIRS observations in several regions of the winter subtropical and northern summer subtropical stratospheres as well. This is likely related, in part, to the GWs generated by sources other than convection, which the particular convective GW parameterization cannot represent. It may also be due to some assumptions considered in the current parameterization, such as ignoring horizontal refraction, the lack of ground-based frequency modulation, and relatively short lifetime of the rays. A number of previous studies showed that the horizontal refraction and frequency modulation along ray trajectories can modify the GW momentum flux significantly [e.g., *Chen et al.*, 2005; *Durran*, 2009]. The lifetime of rays is imposed in the parameterization purely for practical purposes to handle the number of rays, which become far too numerous without any limitation (i.e., generally more than several millions at each time globally). Even in the present offline calculation, the lifetime limit is still required technically, mainly due to handling the dimensions. Although determination of the lifetime of rays is not straightforward, more than 1 day may be recommended, considering that convective GWs generated from the tropics and subtropics propagate into the midlatitudes and even polar regions of the middle atmosphere [*Ern et al.*, 2011]. Impacts of relaxing the three assumptions of the parameterization on performance, and the realism of the parameterized GWTV compared with satellite observations, remain to be examined in future research.

[40] Another feasible way to improve the current convective GW parameterization is to provide a better reality on the diabatic forcing. In the current parameterization, we use an identical spatial/temporal structure of diabatic forcing in both tropics and subtropics, although with different diabatic heating rate at each model grid, and thus similar scales of GWs are launched in the tropics and subtropics. This assumption need to be relaxed, possibly with an information on the characteristics of convective storms in the tropics and subtropics from the satellite observations. From the modeling point of view, any information on the spatial/temporal size of diabatic forcing is not given from the current cumulus parameterization schemes. Perhaps, mesoscale simulation results of the convective storms in GCMs from the superparameterization [e.g., *Khairoutdinov and Randall*, 2001] may be utilized to determine the spatial/temporal structure of diabatic forcing in the tropics and subtropics. Note that the cloud top momentum flux spectra in the tropics and subtropics are different from each other, regardless of the identical diabatic forcing structure, owing to the wave-filtering-and-resonance factor that is another factor to determine the cloud top momentum flux spectrum besides diabatic forcing.

[41] Finally, it is noteworthy that the ray-based parameterization used here is much more realistic than commonly used columnar parameterizations that consider only vertical propagation. The previous studies by *Song and Chun* [2008] and *Choi et al.* [2009] showed that the differences between the ray-based and columnar CGWD parameterizations are significant, especially in the stratospheric equatorial regions.

[42] **Acknowledgments.** This work was funded by the Korean Meteorological Administration Research and Development Program under grant RACS_2010–2008. The ECMWF ERA-Interim data used in this study were obtained from the ECMWF data server. The NCEP DCH data for this study were obtained from the Research Data Archive (RDA) which is maintained by the Computational and Information Systems Laboratory at the National Center for Atmospheric Research (NCAR). NCAR is sponsored by the National Science Foundation. The original data are available from the RDA (http://dss.ucar.edu) in data set ds091.0.

References

Alexander, M. J., et al. (2010), Recent developments in gravity-wave effects in climate models and the global distribution of gravity-wave momentum flux from observations and models, *Q. J. R. Meteorol. Soc.*, *136*, 1103–1124.

Beres, J. H. (2004), Gravity wave generation by a three-dimensional thermal forcing, *J. Atmos. Sci.*, *61*, 1805–1815, doi:10.1175/1520-0469(2004)061<1805:GWGBAT>2.0.CO;2.

Chen, C.-C., D. R. Durran, and G. J. Hakim (2005), Mountain-wave momentum flux in an evolving synoptic-scale flow, *J. Atmos. Sci.*, *62*, 3213–3231, doi:10.1175/JAS3543.1.

Choi, H.-J., and H.-Y. Chun (2011), Momentum flux spectrum of convective gravity waves. Part I: An update of a parameterization using mesoscale simulations, *J. Atmos. Sci.*, *68*, 739–759, doi:10.1175/2010JAS3552.1.

Choi, H.-J., H.-Y. Chun, and I.-S. Song (2009), Gravity wave temperature variance calculated using the ray-based spectral parameterization of convective gravity waves and its comparison with Microwave Limb Sounder observations, *J. Geophys. Res.*, *114*, D08111, doi:10.1029/2008JD011330.

Chun, H.-Y., and J.-J. Baik (1998), Momentum flux by thermally induced internal gravity waves and its approximation for large-scale models, *J. Atmos. Sci.*, *55*, 3299–3310, doi:10.1175/1520-0469(1998)055<3299:MFBTII>2.0.CO;2.

Chun, H.-Y., and J.-J. Baik (2002), An updated parameterization of convectively forced gravity wave drag for use in large-scale models, *J. Atmos. Sci.*, *59*, 1006–1017, doi:10.1175/1520-0469(2002)059<1006:AUPOCF>2.0.CO;2.

Chun, H.-Y., H.-J. Choi, and I.-S. Song (2008), Effect of nonlinearity on convectively forced internal gravity waves: Application to a gravity wave drag parameterization, *J. Atmos. Sci.*, *65*, 557–575, doi:10.1175/2007JAS2255.1.

Dhaka, S. K., M. K. Yamamoto, Y. Shibagaki, H. Hashiguchi, M. Yamamoto, and S. Fukao (2005), Convection-induced gravity waves observed by the Equatorial Atmosphere Radar (0.20°S, 100.32°E) in Indonesia, *Geophys. Res. Lett.*, *32*, L14820, doi:10.1029/2005GL022907.

Durran, D. R. (2009), Comment on "Gravity wave refraction by three-dimensionally varying winds and the global transport of angular momentum," *J. Atmos. Sci.*, *66*, 2150–2152, doi:10.1175/2008JAS3013.1.

Ern, M., P. Preusse, M. J. Alexander, and C. D. Warner (2004), Absolute values of gravity wave momentum flux derived from satellite data, *J. Geophys. Res.*, *109*, D20103, doi:10.1029/2004JD004752.

Ern, M., P. Preusse, J. C. Gille, C. L. Hepplewhite, M. G. Mlynczak, J. M. Russell III, and M. Riese (2011), Implications for atmospheric dynamics derived from global observations of gravity wave momentum flux in stratosphere and mesosphere, *J. Geophys. Res.*, *116*, D19107, doi:10.1029/2011JD015821.

Fritts, D. C., and H.-G. Chou (1987), An investigation of the vertical wavenumber and frequency spectra of gravity wave motions in the lower stratosphere, *J. Atmos. Sci.*, *44*, 3610–3624, doi:10.1175/1520-0469(1987)044<3610:AIOTVW>2.0.CO;2.

Gong, J., D. L. Wu, and S. D. Eckermann (2011), Gravity wave variances and propagation derived from AIRS radiances, *Atmos. Chem. Phys. Discuss.*, *11*, 11,691–11,738, doi:10.5194/acpd-11-11691-2011.

Grimsdell, A. W., M. J. Alexander, P. T. May, and L. Hoffmann (2010), Model study of waves generated by convection with direct validation via satellite, *J. Atmos. Sci.*, *67*, 1617–1631, doi:10.1175/2009JAS3197.1.

Hoffmann, L., and M. J. Alexander (2010), Occurrence frequency of convective gravity waves during the North American thunderstorm season, *J. Geophys. Res.*, *115*, D20111, doi:10.1029/2010JD014401.

Jiang, J. H., S. D. Eckermann, D. L. Wu, and J. Ma (2004a), A search for mountain waves in MLS stratospheric limb radiances from the winter Northern Hemisphere: Data analysis and global mountain wave modeling, *J. Geophys. Res.*, *109*, D03107, doi:10.1029/2003JD003974.

Jiang, J. H., B. Wang, K. Goya, K. Hocke, S. D. Eckermann, J. Ma, D. L. Wu, and W. G. Read (2004b), Geographical distribution and interseasonal variability of tropical deep convection: UARS MLS observations and analyses, *J. Geophys. Res.*, *109*, D03111, doi:10.1029/2003JD003756.

Kanamitsu, M., W. Ebisuzaki, J. Woollen, S.-K. Yang, J. J. Hnilo, M. Fiorino, and G. L. Potter (2002), NCEP-DEO AMIP-II Reanalysis (R-2), *Bull. Am. Meteorol. Soc.*, *83*, 1631–1643, doi:10.1175/BAMS-83-11-1631.

Khairoutdinov, M. F., and D. A. Randall (2001), A cloud-resolving model as a cloud parameterization in the NCAR Community Climate System Model: Preliminary results, *Geophys. Res. Lett.*, *28*, 3617–3620, doi:10.1029/2001GL013552.

Kim, Y.-J., and H.-Y. Chun (2005), A computationally efficient nonstationary convective gravity-wave drag parameterization for global atmospheric prediction systems, *Geophys. Res. Lett.*, *32*, L22805, doi:10.1029/2005GL024572.

Kim, Y.-J., S. D. Eckermann, and H.-Y. Chun (2003), An overview of the past, present, and future of gravity-wave drag parameterization for numerical climate and weather prediction models, *Atmos. Ocean*, *41*, 65–98, doi:10.3137/ao.410105.

Lighthill, J. (1978), *Waves in Fluid*, 539 pp., Cambridge Univ. Press, New York.

Lindzen, R. S. (1981), Turbulence and stress owing to gravity wave and tidal breakdown, *J. Geophys. Res.*, *86*, 9707–9714, doi:10.1029/JC086iC10p09707.

McLandress, C. (1998), On the importance of gravity waves in the middle atmosphere and their parameterization in general circulation models, *J. Atmos. Sol. Terr. Phys.*, *60*, 1357–1383, doi:10.1016/S1364-6826(98)00061-3.

McLandress, C., M. J. Alexander, and D. L. Wu (2000), Microwave Limb Sounder observations of gravity waves in the stratosphere: A climatology and interpretation, *J. Geophys. Res.*, *105*, 11,947–11,967, doi:10.1029/2000JD900097.

Preusse, P., G. Eidmann, S. D. Eckermann, B. Schaelerl, R. Spang, and D. Offermann (2001), Indications of convectively generated gravity waves in CRISTA temperatures, *Adv. Space Res.*, *27*, 1653–1658, doi:10.1016/S0273-1177(01)00231-9.

Preusse, P., S. D. Eckermann, M. Ern, J. Oberheide, R. H. Picard, R. G. Roble, M. Riese, J. M. Russell III, and M. G. Mlynczak (2009), Global ray tracing simulations of the SABER gravity wave climatology, *J. Geophys. Res.*, *114*, D08126, doi:10.1029/2008JD011214.

Ratnam, M. V., G. Tetzlaff, and C. Jacobi (2004), Global and seasonal variations of stratospheric gravity wave activity deduced from the CHAMP/GPS satellite, *J. Atmos. Sci.*, *61*, 1610–1620, doi:10.1175/1520-0469(2004)061<1610:GASVOS>2.0.CO;2.

Richter, J. H., F. Sassi, and R. R. Garcia (2010), Toward a physically based gravity wave source parameterization in a general circulation model, *J. Atmos. Sci.*, *67*, 136–156, doi:10.1175/2009JAS3112.1.

Simmons, A., S. Uppala, D. Dee, and S. Kobayashi (2006), ERA-Interim: New ECMWF reanalysis products from 1989 onwards, *ECMWF Newsl.*, *110*, 25–35.

Song, I.-S., and H.-Y. Chun (2005), Momentum flux spectrum of convectively forced internal gravity waves and its application to gravity wave drag parameterization, Part I: Theory, *J. Atmos. Sci.*, *62*, 107–124, doi:10.1175/JAS-3363.1.

Song, I.-S., and H.-Y. Chun (2008), A Lagrangian spectral parameterization of gravity wave drag induced by cumulus convection, *J. Atmos. Sci.*, *65*, 1204–1224, doi:10.1175/2007JAS2369.1.

Song, I.-S., H.-Y. Chun, and T. P. Lane (2003), Generation mechanisms of convectively forced internal gravity waves and their propagation to the stratosphere, *J. Atmos. Sci.*, *60*, 1960–1980, doi:10.1175/1520-0469(2003)060<1960:GMOCFI>2.0.CO;2.

Song, I.-S., H.-Y. Chun, R. R. Garcia, and B. A. Boville (2007), Momentum flux spectrum of convectively forced internal gravity waves and its application to gravity wave drag parameterization, Part II: Impacts in a GCM (WACCM), *J. Atmos. Sci.*, *64*, 2286–2308, doi:10.1175/JAS3954.1.

Trier, S. B., W. C. Skamarock, M. A. Lemone, D. B. Parsons, and D. P. Jorgensen (1996), Structure and evolution of the 22 February 1993 TOGA COARE squall line: Numerical simulations, *J. Atmos. Sci.*, *53*, 2861–2886, doi:10.1175/1520-0469(1996)053<2861:SAEOTF>2.0.CO;2.

Wang, L., and M. J. Alexander (2010), Global estimates of gravity wave parameters from GPS radio occultation temperature data, *J. Geophys. Res.*, *115*, D21122, doi:10.1029/2010JD013860.

Wright, C. J., and J. C. Gille (2011), HIRDLS observations of gravity wave momentum fluxes over the monsoon regions, *J. Geophys. Res.*, *116*, D12103, doi:10.1029/2011JD015725.

Wu, D. L., and S. D. Eckermann (2008), Global gravity wave variances from aura MLS: Characteristics and interpretation, *J. Atmos. Sci.*, *65*, 3695–3718, doi:10.1175/2008JAS2489.1.

Wu, D. L., P. Preusse, S. D. Eckermann, J. H. Jiang, M. T. Juarez, L. Coy, and D. Y. Wang (2006), Remote sounding of atmospheric gravity waves with satellite limb and nadir techniques, *Adv. Space Res.*, *37*, 2269–2277, doi:10.1016/j.asr.2005.07.031.

Yan, X., N. Arnold, and J. Remedios (2010), Global observations of gravity waves from High Resolution Dynamics Limb Sounder temperature measurements: A yearlong record of temperature amplitude and vertical wavelength, *J. Geophys. Res.*, *115*, D10113, doi:10.1029/2008JD011511.

H.-J. Choi and H.-Y. Chun, Department of Atmospheric Sciences, Yonsei University, 50 Yonsei-ro, Seodaemun-ku, Seoul 120-749, South Korea. (chunhy@yonsei.ac.kr)

J. Gong, Jet Propulsion Laboratory, California Institute of Technology, 4800 Oak Grove Ave., M/S 183-501, Pasadena, CA 91109, USA.

D. L. Wu, NASA Goddard Space Flight Center, MC 613.2, Bldg. 33, Rm. C313, Greenbelt, MD 20771, USA.